predict a significantly larger energy difference for $E(C_{7,eq}) - E(C_{7,ax})$ than most of the force fields (except ECEPP; see Table VII). The hydrogen bond in $C_{7,ax}$ is calculated to be shorter than in $C_{7,eq}$. This is in agreement at least with the CVFF force field, which also predicts a shorter hydrogen bond for $C_{7,ax}$. In the CVFF force field, this is achieved at the expense of unfavorable contributions from angle bending. It apears that, in the $C_{7,ax}$ conformer, the hydrogen bond is pushed together by intramolecular strain.

It is difficult to track down the origins of the force field deficiencies. The analysis that we have carried out so far indicates that several small deviations in various terms of the force field add up to the significant energy differences described above. To be more specific, we would like to point to some possible origins for the descrepancies between ab initio data and at least some of the force fields:

(1) The ab initio data predict similar hydrogen bond lengths $R_{H18\cdots O5}$ for the C_5 and the C_7 conformers. In contrast, both the CVFF and the AMBER force fields give a longer hydrogen bond for C_5 than for C_7. In the CVFF force field, this is at least in part due to deviations in the bond and angle terms. CVFF calculates similar values of R_{N7C9} for the C_5 (1.482 Å) and the C_7 conformers (1.485 Å) of diglycine whereas the ab initio data predict a significantly shorter N7–C9 bond length of 1.434 Å for the C_5 conformer than for the C_7 conformer (1.450 Å). CVFF also calculates similar values of $\angle_{N7C9C12}$ for the C_5 (115.5°) and the C_7 (115.7°) conformers of diglycine whereas the ab initio DZP data predict a $\angle_{N7C9C12} = 109.4°$ for the C_5 conformer and 112.5° for the C_7 conformer. The same trend is found for dialanine. Apparently the CVFF force field underestimates the dependence of the bond length N7–C9 and the angle N7–C9–C12 on conformational change. As the values for R_{N7C9} (C_5, 1.451 Å; C_7, 1.457 Å) and $\angle_{N7C9C12}$ (C_5, 108.5°; C_7, 111.6°) calculated with the AMBER force field[23] for the C_5 and C_7 conformers are in better agreement with the present ab initio data, the origin of the discrepancy must be different. We suspect that the hydrogen bond term in the AMBER force field does not describe accurately the difference between these two conformers. An analysis of the various energy terms of the AMBER force field shows indeed that the hydrogen bond term shows the largest energy differences between the C_5 and the C_7 conformers.

(2) All major current force fields use fixed partial charges that do not change upon conformational changes. However, the present data demonstrate that there is a certain change of partial charges on conformational change. If this charge variation is ignored, the error introduced into the force field is around 1–2 kJ/mol.

In summary, we have shown that ab initio SCF calculations at the DZP level on small model dipeptides can be used to assess the quality of current force fields. The ab initio results point to some important deficiencies of the force fields with respect to the relative energies of the C_7 and the C_5 conformations of dialanine and diglycine. We conclude that several of the current force fields overestimate the stability of the C_7 conformation. We are currently using the present results together with additional ab initio calculations to derive an improved parameter set for a protein force field.

Registry No. Dialanine, 19701-83-8; diglycine, 7606-79-3.

Substituent Effects and the Charge Topology in Nitriles and Cyanides

Yosslen Aray,[†,‡] Juan Murgich,*[,‡] and Miguel A. Luna[§]

Contribution from the Centro de Química, Instituto Venezolano de Investigaciones Científicas (IVIC), Apartado 21827, Caracas 1020A, Venezuela, and Centro Científico, IBM de Venezuela C.A., Apartado 64778, Caracas 1060, Venezuela. *Received June 4, 1990*

Abstract: In order to study the substituent effects and the bonding of the C≡N group, a SCF 4-31G** ab initio calculation was undertaken for the $C{\equiv}N^-$ ion, for nitriles with R = H, F, HO, FO, H_3C, HC≡C, NH_2, O═N, N_3, C≡N, the *E* and *Z* form of iminoacetonitrile and for cyanides with R = Li, HBe, and B. The electron density $\rho(r)$ was analyzed by means of the topological theory of atoms in molecules. The surfaces of zero-flux in $\nabla\rho(r)$ showed that the C valence density of the target fragment absorbed most of the changes, while the N was only slightly perturbed by the R–C bond formation. A correlation was found between the position of the bond critical point and the electronegativity of R for R–C in nitriles but not for the C≡N bond. This difference was explained by the changes in the strength of the substituent fields acting on both bonds. The $\nabla^2\rho(r)$ distribution in the C≡N group for the different substituents and counterions showed that all the bonded and nonbonded local concentrations present in the C and N valence shells were affected in a complex way by the bond formation.

Introduction

One of the most important concepts of chemistry is that rates and equilibria are markedly affected by changes in the molecular skeleton or by the introduction of additional substituents.[1,2] Then, a detailed study of the electronic effects of substitution and coordination on a particular molecular fragment will help to understand the effects governing its chemical behavior. Most of the analyses of the electronic substituent effects were based in the use of σ and π molecular orbitals and their respective populations.[3] This approach is not the most appropriate because molecular orbitals and its population do not constitute physical observables as defined by quantum mechanics.[4,5] An analysis based on a specific orbital description is then flawed by the dependence of the parameters such as the Mulliken population on the model used. In view of these severe limitations, it is more convenient and

[†] On leave from Departamento de Química, Facultad Experimental de Ciencias, Universidad del Zulia, Maracaibo, Venezuela
[‡] Instituto Venezolano de Investigaciones Científicas.
[§] IBM de Venezuela C.A.

(1) Isaacs, N. S. *Physical Organic Chemistry*; Longman Ltd.: Essex, England, 1987; pp 114–170.
(2) Taft, R. W.; Topsom, R. D. *Prog. Phys. Org. Chem.* **1987**, *16*, 1–83.
(3) Topsom, R. D. *Acc. Chem. Res.* **1983**, *16*, 292–298 and *Prog. Phys. Org. Chem.* **1987**, *16*, 85–124.
(4) Bader, R. F. W.; Nguyen-Dang, T. I.; Tal, Y. *Rep. Prog. Phys.* **1981**, *44*, 895–948. Bader, R. F. W. *Atoms in Molecules: a Quantum Theory*; Oxford University Press: Oxford, England, 1990; Chapter 7.
(5) Bader, R. F. W. *Acc. Chem. Res.* **1985**, *18*, 9–15.

0002-7863/91/1513-7135$02.50/0

rigorous to use a physical observable such as the electronic charge density $\rho(r)$ in the analysis of the substituent effects.

It is known that the topology of $\rho(r)$ shows maxima at the position of the nuclei, and no evidence of any shell is found in it.[4-9] Different methods have been used in order to extract information of chemical interest directly from $\rho(r)$. Nevertheless, all the methods had to face the problem that the rearrangements produced by the substituents are very small when compared with $\rho(r)$. This problem led some authors to introduce a hypothetical molecule formed by noninteracting atoms[10] (promolecule). Information about the changes in $\rho(r)$ were then obtained from the difference between the density of the promolecule and that of the calculated molecule.[10] Unfortunately, this approach presents the problem of choosing (or guessing) the correct electronic state of each of the noninteracting atoms that form the promolecule. In many cases, the choice of the electronic states is ambiguous so the results are affected by this uncertainty. Clearly, methods based in other properties of $\rho(r)$ and that do not require the use of hypothetical molecules are needed in an analysis of the substituent effects. In this regard, the differential methods are the most convenient because the changes in $\rho(r)$ will be enhanced and thus easier to determine and locate in space.[4,5] Particularly, the Laplacian $\nabla^2\rho(r)$ readily identifies the atomic regions wherein the electronic charge is locally concentrated or depleted thus providing a much enhanced view of the local form[4-9] of $\rho(r)$. This is a valuable help in the study of substituent effects because the use of the $\nabla^2\rho(r)$ distribution allows the visualization of the density rearrangements *directly* in the three-dimensional space.

It has been shown that the spherical valence shell described by the $\nabla^2\rho(r)$ in an isolated atom is perturbed upon chemical combination, and local extremes are created on it.[4-9] When an atomic group is formed, a set of characteristic extremes is generated in each of the valence shells. Further bonding modifies these extremes and produces changes in $\rho(r)$ that constitute the electronic substituent effects. Therefore, the study of the changes in the $\nabla^2\rho(r)$ distribution in a series of compounds containing a target group allows the direct visualization of the substituent effects in the three-dimensional space. Moreover, the results obtained from a physical observable such as $\rho(r)$ are model independent and do not contain any assumption of dubious physical meaning.[4,5] The previous papers that dealt with the substituent effects in nitriles were written either from the point of view of only the energetics of the substitution process[11] or its conclusions about the changes in $\rho(r)$ were tied to the use of a particular sets of orbitals.[12-14] In the paper by Marriott et al.,[11] the effect of the basis set on the proton-transfer energies was studied in detail for an extensive series of nitriles. The relative gas-phase proton affinities obtained showed an excellent agreement with the experimental values, except for some substituents which exerted large field effects. The work by Marriott et al.[11] was entirely focused on the study of the changes in the total energy of the molecule and its protonated form for different substituents. No information about the changes in the electronic distribution of the target group by the substituents was provided for either form of the nitriles. As the charge distribution in the target group provides important information about its chemical reactivity,[1,2] a study of the topology of $\rho(r)$ for different unprotonated nitriles and cyanides will contribute to the understanding of the chemistry of the C≡N group. In order to determine the modifications introduced in the charge distribution of the C≡N group, a study of the topology of $\rho(r)$ of this fragment was undertaken in present work. The substituent effects on the target group were obtained from the changes in the $\nabla^2\rho(r)$ distribution of the C and N valence shells, the variation in their interatomic surfaces of zero flux in $\nabla\rho(r)$ and in the C and N atomic charges and dipole moments. In order to obtain information about the type of bonding of the C≡N group in ionic and covalently bonded compounds, we have studied also the topology of $\rho(r)$ at the critical point in the R–C and C≡N bonds in a series of nitriles and cyanides.

Computational Methods

The ab initio MO calculations were performed in an IBM 3081 computer with the MONSTERGAUSS program[15] with a 4-31G** basis set and standard exponents and factors.[16] Experimental values for the bond lengths and bond angles were used when available.[17] For R = Li, HO, HCO, (*E*)- and (*Z*)-iminoacetonitrile (IACN), optimized geometries already reported[18] were used while for R = FO, an optimized geometry with a STO-3G set was employed. The topological properties of the charge density and its Laplacian were calculated with a locally modified version of the AIMPAC package.[19]

The basis set dependence of the topological parameters was tested by comparing the values obtained by means of sets of increasing complexity on representative nitriles and cyanides. Different topological properties for R = H, B, N≡C, N=O, F, CH_3, NH_2, and HC=O were calculated with[16,20] a 4-31G**, a 6-31G**, and a triple ζ basis set with double polarization functions[21] at the known molecular geometry. As expected, the position of the critical point r_c and $\rho(r_c)$ in the R–C and C≡N bonds showed little variation with the basis set change. A linear correlation between the values of the principal components of the $\nabla^2\rho(r)$ calculated with the 4-31G** and with the more complex sets was found for the R–C and C≡N bonds with $0.964 \le r \le 0.997$. A similar correlation for the $\nabla^2\rho(r)$ values at the maxima and saddle points found in the C≡N bond and in the valence shell of the C and N atoms gave even higher values ($0.981 \le r \le 0.997$). Therefore, the trends found with the more complex sets seem to be accurately reflected in the 4-31G** values. This fact, together with the required economy in computer time, led us to adopt the smaller set in our work. For LiCN, a much more complex basis set is required[22] so only the topology of the bonds was analyzed with the LiCN configuration, and the results are expected to be at least of qualitative value.

Theory

The topological properties of $\rho(r)$ are displayed by its $\nabla\rho(r)$ and $\nabla^2\rho(r)$ fields.[4-9] Every gradient path originates and terminates at a critical point in $\rho(r)$ where $\nabla\rho(r) = 0$; these points are classified by the three eigenvalues λ_i (i = 1, 2, and 3) of the Hessian matrix ($H_{ij} = \partial^2\rho(r)/\partial x_i \partial x_j$). In the nitriles studied here, only two types of critical points exist that labeled by their rank (number of nonzero eigenvalues) and signature[4-9] (excess number of positive over negative eigenvalue) are (3,–1) and 3,–3). A (3,–3) point is a local maximum, while a (3,–1) represents local maxima in two directions and a local minimum in the third one and is called a bond critical point. The (3,–3) points occur generally at the nuclear positions so that each nucleus is a three-dimensional point attractor in the vector field spanned[4-9] by $\nabla\rho(r)$. The region transversed by the gradient paths which terminate at a given attractor is called the basin of the attractor. The unique trajectory

(6) Bader, R. F. W.; Essen, H. *J. Chem. Phys.* **1984**, *80*, 1943–1959.
(7) Bader, R. F. W.; MacDougall, P. J.; Lau, C. D. H. *J. Am. Chem. Soc.* **1984**, *106*, 1594–1605.
(8) Bader, R. F. W.; MacDougall, P. J. *J. Am. Chem. Soc.* **1985**, *107*, 6788–6795.
(9) Wiberg, K. B.; Bader, R. F. W.; Lau, C. D. H. *J. Am. Chem. Soc.* **1987**, *109*, 985–1001, 1001–1012.
(10) Coppens, P. *J. Phys. Chem.* **1989**, *93*, 7979–7984.
(11) Marriott, S.; Topsom, R. D.; Lebrilla, C. B.; Koppel, I.; Mishima, M.; Taft, R. W. *J. Mol. Struct.* **1986**, *137*, 133–141.
(12) Aray, Y.; Gomperts, R.; Soscun, H.; Murgich, J. *THEOCHEM* **1984**, *180*, 223–229.
(13) Nalin, C. J.; Bagus, P. S.; Philpott, M. R. *J. Chem. Phys.* **1987**, *87*, 2170–2176.
(14) Rodriguez, J. A.; Campbell, C. T. *Surf. Sci.* **1987**, *187*, 299–318.
(15) MONSTERGAUSS 86 is a version of MONSTERGAUSS 82 modified by R. Bonaccorsi, Istituto di Chimica Quantistica del C.N.R., Pisa, Italy.
(16) Ditchfield, R.; Hehre, W. J.; Pople, J. A. *Chem. Phys.* **1970**, *54*, 724.
(17) Data for HCN and CH_3CN: Constain, C. C.; Stoichef, B. P. *J. Chem. Phys.* **1959**, *30*, 777–782. For FCN and HCCCN: Tyler, J. K.; Sheridan, J. *Trans. Faraday Soc.* **1963**, *59*, 2661–2670. For NH_2CN: Tyler, J. K.; Sheridan, J.; Constain, C. C. *J. Mol. Spectrosc.* **1972**, *43*, 248–261. For NCCN: Morino, Y.; Kuchitsu, K.; Yori, Y.; Tamimoto, M. *Bull. Chem. Soc. Jpn.* **1968**, *41*, 2349–2352. For HOCN and FOCN: Poppinger, D.; Radom, L. *J. Am. Chem. Soc.* **1978**, *101*, 3674–3685. For HCOCN: Eiseinstein, M.; Hirshfeld, F. L. *J. Comput. Chem.* **1983**, *2*, 15–22.
(18) Aray, Y.; Murgich, J. *J. Chem. Phys.* **1989**, *91*, 293–299.
(19) Biegler-Konig, F. W.; Bader, R. F. W.; Nguyen-Dang, T. T. *J. Comp. Chem.* **1982**, *3*, 317–323.
(20) Binkley, J. S.; Pople, J. A.; Hehre, W. J. *J. Am. Chem. Soc.* **1980**, *102*, 939–947. Gordon, M. S.; Binkley, J. S.; Pople, J. A.; Pietro, W. J.; Hehre, W. J. *J. Am. Chem. Soc.* **1982**, *104*, 2797–2803.
(21) Clementi, E.; Corongiu, G. *Chem. Phys. Lett.* **1982**, *90*, 359–364.

Table I. Position, Charge Density, and Topological Characteristics at the Critical Point of the C≡N Bond[a,b]

R	$-Z$	$-\lambda_1$	$-\lambda_2$	λ_3	$\rho(r_c)$	$\nabla^2\rho(r_c)$	$\lvert\lambda_1\rvert/\lambda_3$	ϵ
C≡N⁻	0.752	1.186	1.186	2.680	0.445	0.307	0.443	0.000
Li	0.733	1.274	1.274	3.253	0.492	0.705	0.392	0.000
HBe	0.740	1.149	1.149	2.960	0.480	0.663	0.388	0.000
B	0.733	1.189	1.189	3.229	0.497	0.852	0.368	0.000
F	0.752	0.724	0.724	2.208	0.458	0.761	0.328	0.000
HO	0.750	0.831	0.794	2.350	0.462	0.726	0.354	0.044
FO	0.748	0.810	0.754	2.406	0.459	0.841	0.337	0.074
H	0.745	0.997	0.997	2.699	0.475	0.704	0.369	0.000
H_3C	0.748	1.000	1.000	2.568	0.475	0.568	0.389	0.000
HC≡C	0.749	0.970	0.970	2.536	0.473	0.596	0.383	0.000
N≡C	0.749	0.933	0.933	2.509	0.468	0.643	0.372	0.000
(*E*)-IACN	0.747	1.000	0.990	2.617	0.474	0.627	0.382	0.010
(*Z*)-IACN	0.747	1.005	0.995	2.623	0.475	0.623	0.383	0.010
HC=O	0.750	0.977	0.977	2.534	0.468	0.581	0.386	0.000
NH_2	0.753	0.938	0.860	2.337	0.468	0.538	0.401	0.091
O=N	0.740	0.979	0.968	2.829	0.484	0.882	0.346	0.011
N_3	0.749	0.917	0.868	2.430	0.471	0.646	0.377	0.056

[a] All quantities are in atomic units. [b] The values for R = B, H, CN, CCH, CH_3, F, (*Z*)-IACN, HCO, NH_2, HO, and FO were reported: Aray, Y.; Murgich, J. *J. Chem. Phys.* **1989**, *91*, 293–299.

traced out by $\nabla\rho(r)$ and associated with the positive eigenvalue of the Hessian (λ_3) in a (3,−1) point connects two bonded atoms and defines the bond path. The trajectories associated with the negative eigenvalues (λ_1 and λ_2) at the (3,−1) point define the zero-flux surface that partitions the molecule into unique fragments.[4-9] Therefore, the set of surfaces formed by all (3,−1) points partitions the molecular charge into a collection of chemically identifiable regions called atomic basins. In bonds where the charge is preferentially accumulated in a given plane, the negative curvatures of ρ will differ in value at the critical point; if λ_2 is the smallest curvature, the ellipticity that provides a measure of the asymmetry of that bond is defined[4-9] as $\epsilon = \lambda_1/\lambda_2 - 1$.

Because the $\nabla^2\rho(r)$ provides information about regions wherein the charge distribution is depleted ($\nabla^2\rho(r) > 0$) or accumulated ($\nabla^2\rho(r) < 0$), it has been used to classify the interatomic interactions present in molecules.[6] The values of $\nabla^2\rho(r_c)$ at the bond critical point are negative for a covalent interaction. In such a case, the regions over which $\nabla^2\rho(r) < 0$ contains most of the valence regions of both atoms and leads to a single region of relatively low potential energy.[6] A second type of interatomic interaction (ionic bond) where $\rho(r_c)$ is relatively low and the $\nabla^2\rho(r_c) > 0$ parallels the interaction between closed-shell systems.[6] The regions where the $\nabla^2\rho(r) < 0$ in this case are identical, except for polarization effects, with those found in a free atom or ion. In some bonds called the intermediate or polar type, the critical point is located close to or at the nodal surface in $\nabla^2\rho(r)$ and the basins neighboring the interatomic surface exhibit opposite behavior with respect to the sign of the Laplacian. In this case, $\rho(r_c)$ is large although the $\nabla^2\rho(r_c)$ is positive, while $|\lambda_1|/\lambda_3$ have values intermediate between those found for closed-shell and covalent interactions.[6]

Results and Discussion

Information about the substituent electronic effects are obtained from the comparison of the surfaces of zero-flux in $\nabla\rho(r)$, the extremes in the $\nabla^2\rho(r)$ distribution of a target group, and from the variation of its bond critical points before and after bonding. In Figures 1 and 2 are shown different maps of the $\nabla^2\rho(r)$ for C≡N⁻ and for some representative nitriles and cyanides. The $\nabla^2\rho(r)$ distribution in an isolated light atom shows the existence of a number of alternating pairs of shells of charge depletion and concentration.[7,8] The valence shell in this case is a sphere on whose surface the charge distribution is maximal and, in atoms without nucleus with electric quadrupole moments, uniform. The formation of bonds produces a number of local maxima and minima[7,8] in the valence shell with characteristics that are a function of the intervening atoms (see Figure 2). In the C≡N⁻ ion, the negative field exerted on the C, as a result of the transfer of charge toward the N, polarizes the C valence density toward a region behind the C–N bond where it forms a diffuse and extended distribution both radially and laterally ("lone pair"). Similarly, the formation of the C≡N bond also produces a nonbonding concentration ("lone pair") on the N valence shell (see Figure 2) more tightly bound and larger in magnitude than in the C atom. In contrast[7] with C=O, in the Laplacian distribution of C≡N⁻ there is no torus of charge depletion in the C density encircling the internuclear axis (Figure 2). This torus provides the region for nucleophilic attack in C=O or C=O containing molecules.[7,8] The lack of such a torus in the C≡N group indicates that a nucleophilic attack is less likely in nitriles and cyanides unless regions of charge depletion are generated as in F—C≡N. In this regard, it is known that strong nucleophiles such as carbanions, OH^-, and hydroxylamines are added easily to the C atom in aliphatic nitriles.[23] On the other hand, it has been found experimentally that much weaker nucleophiles may be added only if the nitrile is attacked first by a strong acid.[23] A comparison of the charge distribution of H_3C—C≡N and $(H_3C$—C≡N—H$)^+$ showed[24] that upon protonation, the Laplacian decreased from 0.087 to 0.046 a.u. at the saddle point of the valence shell of the nitrile C atom. The decrease in this density opens the path for a nucleophilic attack[7,8] at the C atom in nitriles and provides an explanation of the acid catalysis found in this class of compounds.[23]

The continuous region of concentration of charge that envelopes both atoms in th C≡N⁻ indicates that such a fragment is a better donor (soft base) and more susceptible to an electrophilic attack than the C=O group.[7,8] The difference in the characteristics of the "lone pairs" explains the soft character of the C atom and the hard one found for the N in the C≡N⁻ ion. The rather extended and diffuse C nonbonded density is more polarizable than the tightly held N "lone pair", and so it is more easily shared with an approaching fragment than the N nonbonded density. For this reason, the C≡N⁻ predominantly bonds with soft acids through the C atom.

In Tables I and II are shown the parameters that characterize the topology of $\rho(r)$ at the critical point in the C≡N and R–C bonds. We see from Table I that both the position of that point and the values of $\rho(r_c)$ in the C≡N show only small fluctuations upon the formation of the R–C bond. The large values of $\rho(r_c)$, the positive $\nabla^2\rho(r_c)$, and the near coincidence of the interatomic surface $S_{C\equiv N}$ with a nodal line of the $\nabla^2\rho(r)$ show[6] that the C≡N bond is of the intermediate type in both the cyanides and nitriles. A comparison between Tables I and II indicates that $\rho(r_c)$ and $\nabla^2\rho(r_c)$ vary between much broader limits in the R–C than in the C≡N bond. The $S_{C\equiv N}$ surface showed only minor changes in its shape while S_{CR} exhibited significant variations upon substitution as seen in Figure 1. When two atoms approach each other,

(22) Adamowicz, L.; Frum, C. I. *Chem. Phys. Lett.* **1989**, *157*, 496–500.
(23) Smith, P. A. S. *Open-Chain Organic Nitrogen Compounds*; W. A. Benjamin: New York, 1965,; Vol. I, p 213.
(24) Aray, Y. Ph.D. Thesis, Centro de Química, Instituto Venezolano de Investigaciones Científicas, Caracas, Venezuela, 1990.

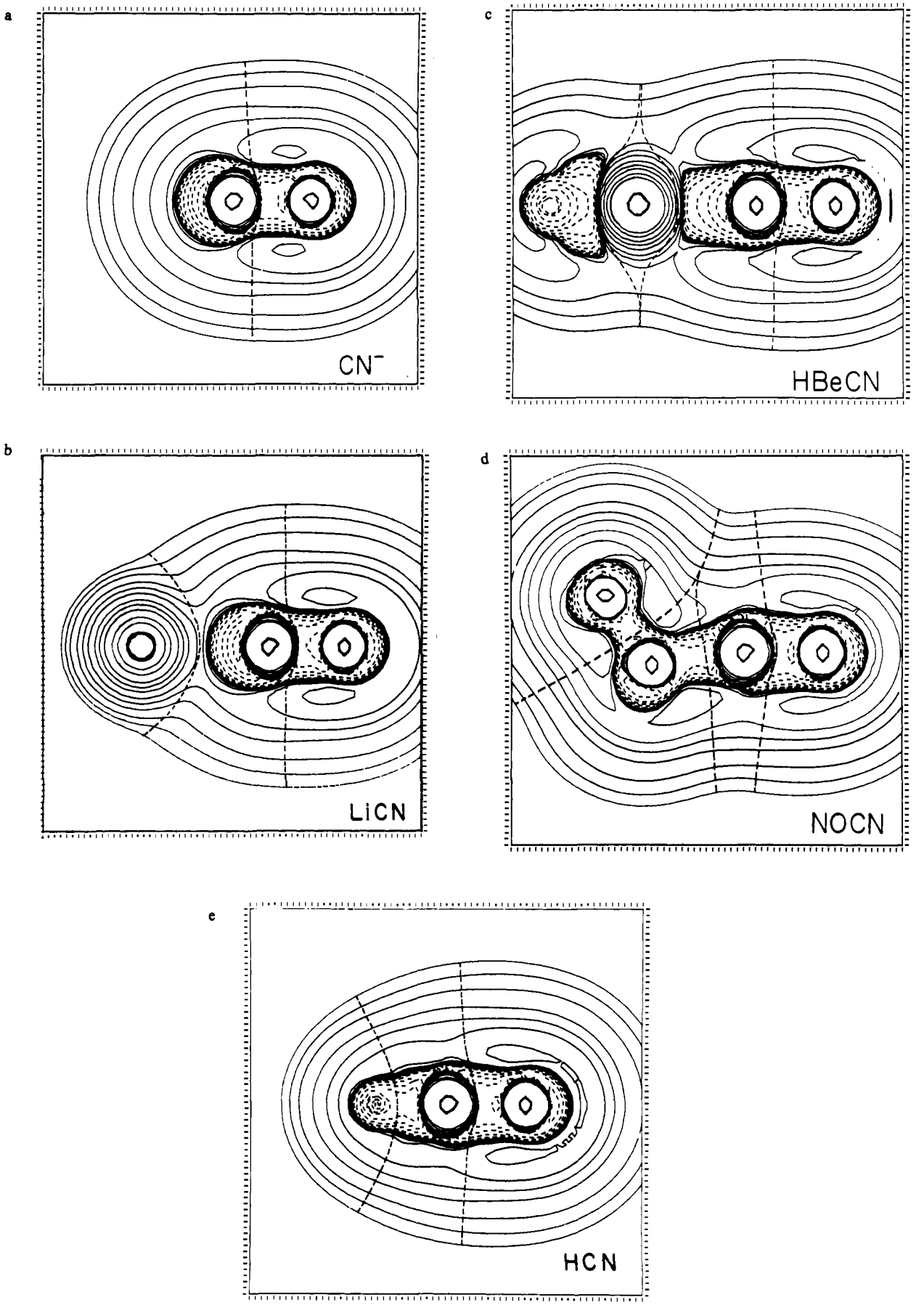

Figure 1. Contour map of the Laplacian of $\rho(r)$ for (a) C≡N⁻, (b) LiC≡N, (c) HBeC≡N, (d) N═OC≡N, and (e) HC≡N, in the nuclear plane. Positive values of $\nabla^2\rho(r)$ are denoted by solid contours, negative values by dashed contours. The contour values in au are ±0.002, ±0.004, ±0.008, increasing in powers of 10 to ±8.0. The outermost contour in each plot is ±0.002 au. The intersection of the zero-flux surface with the nuclear plane is shown as a heavy dashed line.

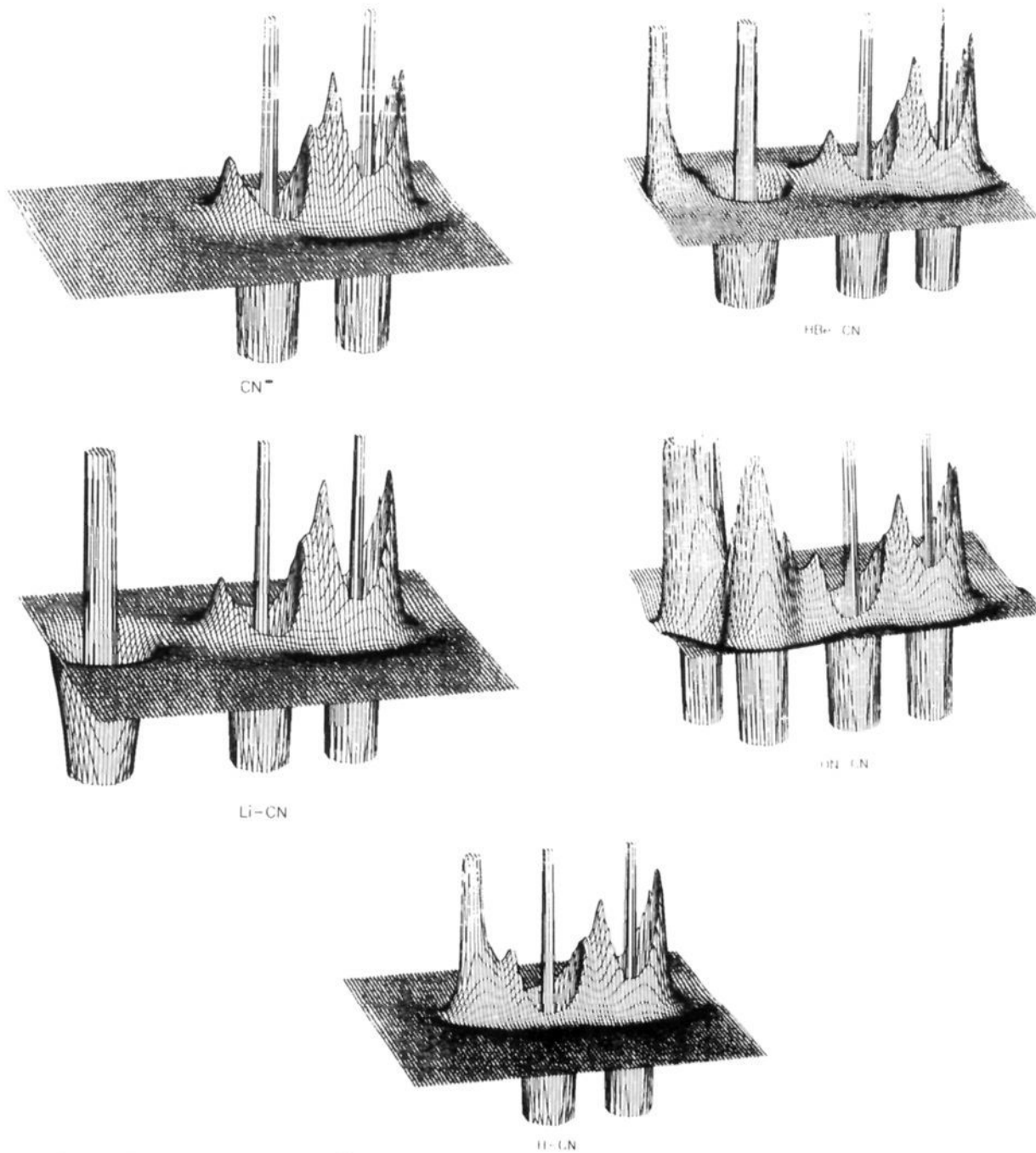

Figure 2. Two-dimensional relief maps of $-\nabla^2\rho(r)$ for some cyanides and nitriles. These relief plots have a cutoff value of ±2.0 au and are all drawn to the same scale. The spike-like feature at the position of the nuclei and the adjacent deficit are regions of charge concentration and depletion, repectively, of the core shells. The second pair of alternating regions of charge concentraton and depletion corresponds to the valence shell.

their basins are modified until the density is such that a balance is achieved at the equilibrium distance. Fragments that produce a net attracting field over the target density are expected then to push the interatomic surface toward the target atom until the equilibrium is reached. Fragments unable to generate such a field will show an opposite behavior (see Figure 1). The electronegativity has been used for many years as indicative of the attracting power of an atom,[25] so it is interesting to explore its relationship with the interatomic surfaces and bond critical points. The electronegativity has been defined as the ability of an atom or group to attract electrons.[25] This definition could be restated as the ability of an atom or fragment to change its charge through the modification of the basin density and/or of its interatomic surfaces. In our study, we could take the position of the bond critical points as representative of the position of the interatomic surfaces and use an electronegativity scale for the different Rs derived from the charge topology of its different hydrides.[26] From plots of this electronegativity vs r_c, we found a linear correlation ($r = 0.964$) between these parameters in the R–C but none in the C≡N bond. From Figure 1, we see that the position of the critical points show much larger changes in the R–C than in the C≡N bond. This result is a consequence of (a) the strong dependence with distance of the substituent field[27] and (b) from the fact that it has to compete with the much stronger nuclear field in bonds other than R–C. For these reasons, in the C≡N bond, the substituent field is only able to perturb its charge distribution in

(25) Pauling, L. *The Nature of the Chemical Bond*, 3rd ed.; Cornell University Press: Ithaca, New York, 1960; pp 89–103.

(26) Boyd, R. J.; Edgecombe, K. E. *J. Am. Chem. Soc.* **1988**, *110*, 4182–4186.

Table II. Position, Charge Density, and Topological Characteristics at the Critical Point of the R–C Bond[a,b]

R	$-Z$	$-\lambda_1$	$-\lambda_2$	λ_3	$\rho(r_c)$	$\nabla^2\rho(r_c)$	$\lvert\lambda_1\rvert/\lambda_3$	ϵ
Li	2.363	0.064	0.064	0.355	0.040	0.227	0.180	0.000
HBe	2.210	0.175	0.175	0.590	0.084	0.241	0.297	0.000
B	2.065	0.431	0.431	0.905	0.164	0.044	0.476	0.000
F	0.777	0.866	0.866	2.601	0.313	0.869	0.333	0.000
HO	0.842	0.736	0.723	1.006	0.305	0.453	0.732	0.018
FO	0.847	0.690	0.685	0.965	0.293	−0.409	0.715	0.006
H	1.315	0.874	0.874	0.393	0.304	−1.354	2.224	0.000
H_3C	1.588	0.533	0.533	0.190	0.275	−0.877	2.805	0.000
HC≡C	1.361	0.645	0.645	0.213	0.318	−1.077	3.028	0.000
N≡C	1.314	0.639	0.639	0.230	0.312	−1.049	2.778	0.000
(*E*)-IACN	1.547	0.573	0.549	0.238	0.276	−0.884	2.408	0.044
(*Z*)-IACN	1.566	0.554	0.539	0.230	0.272	−0.863	2.409	0.028
HC=O	1.530	0.601	0.584	0.251	0.283	−0.934	2.620	0.029
NH_2	0.882	0.804	0.767	0.407	0.342	−1.165	1.975	0.048
O=N	1.105	0.765	0.739	0.249	0.327	−1.255	3.069	0.035
N_3	0.873	0.776	0.744	0.504	0.332	−1.016	1.541	0.043

[a] All quantities are in atomic units. [b] The values for R = B, H, C≡N, C≡CH, CH_3, F, (*Z*)-IACN, HC=O, NH_2, HO, and FO were reported: Aray, Y.; Murgich, J. *J. Chem. Phys.* **1989**, *91*, 293–299.

a way that is not represented by the electronegativity of R. Therefore, the electronegativity seems to be mainly connected with a rather local response of the valence shell of the atom to which the R fragment is attached (vide infra). This limited response explains the rather short range of the inductive effect associated with the differences in electronegativity.[1,2]

For nitriles containing groups such as NH_2, N_3, and HC=O, delocalization of some of its charge distribution along a certain plane ("π conjugation") is expected to occur toward or from[1,2] the C≡N group. Such a delocalization will generate a finite ellipticity in the R–C bond so its density will fall off from its maximum value at r_c more slowly in the plane containing the smallest of the two negative curvatures.[28] For this reason, the ellipticity ϵ has been linked with the classical "double" bond character.[28] As seen in Table II, the ellipticity for the R–C bond ϵ_{RC} was in NH_2 > (*E*)-IACN > N_3 > N=O > (*Z*)-IACN > OH > FO. The low values of ϵ_{RC} (<0.05) compared with ethylene[27] ($\epsilon_{C=C}$ = 0.22) show that the "double" bond character is rather small for R–C in nitriles. The eigenvectors at r_c in R–C showed that the bond charge accumulates perpendicularly to the nuclear plane of the molecule. The symmetry of the C≡N group is perturbed by the delocalization occurring in the R–C bond so a preferential plane will also exist in this bond. This asymmetry could be described by a bond ellipticity as defined above.[28] The ellipticity found for the C≡N bond ϵ_{CN} and shown in Table I was in NH_2 > FO > HO > N_3 > N=O > (*E*)- = (*Z*)-IACN ≫ HC=O. The eigenvectors at r_c showed that charge in the C≡N was accumulated in a plane that was always perpendicular to that found in the R–C bond. The values of ϵ_{CN} (<0.09) indicate again that the asymmetric accumulation is quite noticeable in the C≡N bond. At first sight, one may expect a relationship between the ellipticities of the R–C and C≡N bonds. Nevertheless, from Tables I and II, we see that there is no correlation between these quantities. In particular, in the (*E*)- and (*Z*)-IACN, the target group is perturbed by two slightly different fields as a result of the rotation of a distant H atom. In this case, we know that the ϵ_{CN} values are equal but the ϵ_{RC} differ noticeably (0.044 and 0.028). A source for this lack of correlation may be variations in the local response of the valence densities[29,30] to slightly different substituent fields.

A smooth transition from ionic to polar or intermediate to covalent was observed from the topology of the R–C bond. For H, CH_3, NH_2, HC≡C, C≡N, (*E*)- and (*Z*)-IACN, HC=O, N=O, and N_3, the values of $|\lambda_1|/\lambda_3$, $\rho(r_c)$, and $\nabla^2\rho(r_c)$ (see Table II) for the R–C bond are typical of H–C, N–C, and C–C covalent bonds,[6] while for R = F, OH, and OF, the values are typical of intermediate or polar F–C or O–C bonds.[6] The polar character of the latter bonds was further confirmed by the position of the critical point which is in or very near one of the nodal surfaces of the $\nabla^2\rho(r)$ and by the large values of $\rho(r_c)$ and of $\nabla^2\rho(r_c)$. For R = Li, HBe, and B, $\rho(r_c)$ was quite low indicating that the density is pushed toward each fragment. Also $|\lambda_1|/\lambda_3 < 1$ and the values of $\nabla^2\rho(r_c)$ were positive showing that the R–C bonds[6] were ionic in the latter compounds.

Laplacian of ρ in Cyanides and Nitriles

In order to determine the changes produced by the substituents (or counterions) in other parts of the valence density of the C≡N group, a study of the extremes present in its $\nabla^2\rho(r)$ distribution was undertaken. In Tables III–VII are shown the values and positions obtained for extremes of the density of the valence shells of the C≡N group in several nitriles and cyanides. An inspection of these tables shows that the characteristics of the extremes vary with the type of atom or molecular fragment to which the C≡N is attached. The origin of the local concentrations is a consequence of the partial condensation of the valence electrons into pairs as a result of the localization of the Fermi hole.[31] This localization is a direct result of the combined action of the ligand or substituent field and of the Pauli exclusion principle[31] on $\rho(r)$. In the present case, the formation of the C≡N$^-$ ion produces local concentrations in the valence shell of both the C and the N atoms that are later modified by the additional bonding. The local extremes reflect the spatial variation of the substituent field near its source charges and also the nonlocal character of the polarizability and hyperpolarizability response function of the target density.[29,30] The rapidly varying components of the substituent field are associated with the higher electrical multipoles and are particularly important in the proximity of the source density because a 2^k multipole produces a component that decreases[27] as $R^{-(k+2)}$. Then, the part of the target nearest to the substituent will be affected by a field that contains strong multipolar components, while the distant parts will be mostly perturbed by the more uniform and weaker dipolar (and sometimes monopolar) component.[32] The substituent effects are therefore reflected in the variation of the number and types of the extremes that the external field is able to produce in the target density. In organic chemistry, the substituent effects have been divided somewhat arbitrarily into inductive (or through the bond), resonance, field, and polarization effects.[1,2] Such division does not reflect the fact that all of them are generated by a common cause: the electric field produced by the substituent. The inductive effect is the result of the action of a strong and rapidly varying substituent field where the high multipolar terms may play an important role at short ranges. The resonant, field, and polarization effects, on the other hand, are connected mainly with

(27) Böttcher, C. J. F. *Theory of Electric Polarization*; 2nd ed.; Elsevier: Amsterdam, 1973; pp 8–58.
(28) Bader, R. F. W.; Slee, T. S.; Cremer, D.; Kraka, E. *J. Am. Chem. Soc.* **1983**, *105*, 5061–5068.
(29) Sipe, J. E.; van Kranendok, E. *Mol. Phys.* **1978**, *35*, 1579–1584.
(30) Stone, A. J. *Mol. Phys.* **1985**, *56*, 1065–1082.
(31) Bader, R. F. W.; Stephens, M. E. *J. Am. Chem. Soc.* **1975**, *97*, 7391–7399.
(32) Ghio, G.; Scrocco, E.; Tomasi, J. *Theor. Chim. Acta (Berlin)* **1978**, *50*, 117–134.

Table III. Position and Laplacian at the Maxima and at the Saddle Point of the R–C Bond[a]

R	X	Z	$\nabla^2\rho(r)$	μ_3	signature
C≡N⁻	0.000	−0.897	1.204	68.017	−3
HBe	0.000	−0.930	1.157	51.015	−3
B	0.000	−0.933	1.371	49.940	−3
	0.000	−1.576	0.573	2.695	−1
	0.000	−1.757	0.587	3.229	−3
H	0.000	−0.956	1.505	36.660	−3
	0.000	−1.205	1.261	9.551	−1
H_3C	0.000	−0.951	1.423	41.261	−3
	0.000	−1.446	0.873	4.788	−1
	0.000	−1.745	0.985	20.301	−3
HC≡C	0.000	−0.969	1.407	33.778	−3
	0.000	−1.317	1.069	5.844	−1
N≡C	0.000	−0.978	1.338	30.405	−3
	0.000	−1.314	1.049	5.767	−1
(*E*)-IACN	−0.004	−0.955	1.399	40.000	−3
	−0.001	−1.437	0.851	5.085	−1
(*Z*)-IACN	0.008	−0.953	1.393	40.683	−3
	0.008	−1.446	0.825	4.910	−1
HC=O	0.006	−0.954	1.439	40.418	−3
	−0.003	−1.421	0.899	5.424	−1

[a] All quantities are in atomic units.

Table IV. Position and the Laplacian at the Saddle Points of the Valence Shell of the C Atom[a]

R	X	Y	Z	$\nabla^2\rho(r)$
C≡N⁻	0.978	0.000	0.269	0.083
HBe	0.997	0.000	0.036	0.136
B	0.994	0.000	−0.029	0.131
H	0.965	0.000	−0.248	0.083
H_3C	0.966	0.000	−0.241	0.087
	−0.967	0.000	−0.237	0.085
HC≡C	0.953	0.000	−0.283	0.071
N≡C	0.941	−0.005	−0.315	0.077
(*E*)-IACN	0.957	0.000	−0.278	0.075
	−0.961	0.967	−0.259	0.074
	0.028	0.967	−0.222	0.115
	0.028	−0.967	−0.222	0.115
(*Z*)-IACN	0.963	0.000	−0.250	0.087
	−0.959	0.969	−0.272	0.078
	0.024	0.969	−0.214	0.116
	0.024	−0.969	−0.214	0.116
HC=O	0.963	0.000	−0.259	0.063
	−0.962	0.000	−0.268	0.069
	−0.027	−0.964	−0.217	0.148
	−0.027	0.964	−0.217	0.148

[a] All quantities are in atomic units.

the dipolar part with a smaller contribution from the high multipolar terms. Examples of the effect of the external field may be found in the different parts of the target density. In particular, in the C≡N fragment, when R is attached to the C atom, a strong variation is found in its "lone pair". The $\nabla^2\rho(r)$ distribution shows that its density is driven toward the bond path (see Table III) and its angular spread is drastically reduced (see Figure 2). As a result of this rearrangement, the maximum in $\nabla^2\rho(r)$ increases, while its positive curvature along the R–C axis μ_3 decreases markedly. The increase in $\nabla^2\rho(r)$ at the maximum located near the C atom is the result of the concentration toward the R–C bond path, while the decrease in μ_3 shows that the maximum is now more "rounded" because the density is attracted by additional nuclei. For electron acceptor fragments such as NH_2, N=O, N_3, HO, FO, and F, no maximum was found in the R side of the C basin of the C≡N. On the contrary, on donor fragments such as CH_3, one or more maxima were found in this region as seen in Table III. This is the result of the changes produced in the interatomic surface by the substituent field. The maximum in the C atom of the C≡N in molecules formed with acceptor fragments is incorporated into the basin of the atom of R to which it is bonded, while for the other fragments the opposite is true. The formation of an ionic R–C bond, on the other hand, produces smaller changes in the C "lone pair" although in B—C≡N, a small secondary maximum was found in the C basin in ionic bonds, the polarization of the closed-shell fragments determines their charge distribution.[6] Due to the charge transfer, in B—C≡N the interatomic surface S_{BC} is pushed toward the B atom. Nevertheless, the nuclear field of the B atom is still able to generate a small maximum in that density, while this is not the case in HBe—C≡N.

The formation of the two maxima in the C valence density, one facing R and the other facing the N atom, also produces a set of saddle points and/or mimima over the shell that are located more or less perpendicularly to the C≡N direction (see Figure 2 and Table IV). In linear nitriles, a set of infinite (2,0) saddle points forms a circle around the C–N direction while in the asymmetric ones only two (3,−1) saddle and two (3,+1) critical points are found in the valence shell. In the lattice nitriles, as seen in Table IV, noticeable differences were found in both the position and the value of $\nabla^2\rho(r)$ at each of the saddle points as a result of the transverse component of the substituent field.

The position and the value of the $\nabla^2\rho(r)$ at the extremes in the C≡N interatomic region are shown in Table V. When a bond is formed between two similar atoms, in general a maximum in the density is expected to occur along the bond path near each atomic core (see Figure 2). In the C≡N bond these points are within the N basin as expected from the difference in the electronegativity with the C atom. As seen in Table V, a large

Table V. Position and Laplacian at the Bonded Maxima and at the Saddle Point of the C≡N Bond[a]

R	X	Z	$-\nabla^2\rho(r)$	μ_3	signature
C≡N⁻	0.000	0.974	1.745	30.084	−3
	0.000	1.135	1.638	9.132	−1
	0.000	1.469	2.824	151.536	−3
HBe	0.000	0.999	1.814	11.963	−3
	0.000	1.054	1.808	8.875	−1
	0.000	1.394	2.986	155.526	−3
B	0.000	1.358	3.127	157.651	−3
F	0.000	0.983	1.325	22.065	−3
	0.000	1.094	1.286	4.187	−1
	0.000	1.371	1.916	105.850	−3
HO	0.002	0.984	1.430	21.717	−3
	0.001	1.091	1.394	5.214	−1
	0.003	1.375	2.088	112.716	−3
FO	0.031	0.991	1.408	18.718	−3
	0.018	1.083	1.385	5.119	−1
	0.032	1.380	2.135	117.440	−3
H	0.000	0.999	1.634	11.957	−3
	0.000	1.057	1.628	6.894	−1
	0.000	1.383	2.613	138.622	−3
H_3C	0.000	0.987	1.629	18.774	−3
	0.000	1.075	1.608	7.200	−1
	0.000	1.384	2.525	134.046	−3
HC≡C	0.000	0.990	1.616	17.425	−3
	0.000	1.073	1.598	7.056	−1
	0.000	1.388	2.533	134.333	−3
N≡C	0.000	0.992	1.580	17.127	−3
	0.000	1.076	1.562	6.832	−1
	0.000	1.397	2.546	137.485	−3
(*E*)-IACN	−0.003	0.993	1.633	15.839	−3
	−0.003	1.067	1.620	7.137	−1
	−0.009	1.386	2.586	137.670	−3
(*Z*)-IACN	−0.002	0.993	1.639	15.751	−3
	−0.002	1.067	1.625	7.365	−1
	−0.002	1.386	2.600	138.292	−3
HC=O	0.001	0.991	1.600	17.835	−3
	0.002	1.077	1.580	7.367	−1
	0.006	1.400	2.592	140.037	−3
NH_2	0.003	0.980	1.519	23.114	−3
	0.003	1.092	1.478	6.230	−1
	0.014	1.381	2.230	119.061	−3
O=N	0.033	1.355	2.599	135.857	−3
N_3	0.023	0.986	1.527	19.542	−3
	0.014	1.078	1.503	6.118	−1
	0.025	1.373	2.278	121.530	−3

[a] All quantities are in atomic units.

maximum M_1 is located near the N, while a secondary one M_2 is found near the C core except for R = N=O where only M_1 was found. The disappearance of M_2 in N=O—C≡N may be

Table VI. Position and Laplacian of the Saddle Points of the Valence Shell of the N Atom

R	X	Y	Z	$-\nabla^2\rho(r)$	X	Y	Z	$-\nabla^2\rho(r)$
C≡N⁻	−0.804	0.000	2.128	0.829	0.000	−0.804	2.128	0.829
	0.804					0.804		
HBe	−0.809	0.000	2.053	0.701	0.000	−0.809	2.053	0.701
	0.809					0.809		
B	−0.812	0.000	2.023	0.664	0.000	−0.812	2.023	0.664
	0.812					0.812		
F	−0.788	0.000	1.986	0.880	0.000	−0.788	1.986	0.880
	0.788					0.788		
HO	−0.783	0.014	1.987	0.973	0.000	−0.799	2.005	0.735
	0.783						2.008	0.747
FO	−0.780	0.022	1.989	1.045	0.000	−0.804	1.999	0.606
	0.780					0.808	2.033	0.641
H	−0.805	0.000	2.032	0.742	0.000	−0.805	2.032	0.742
	0.805					0.805		
H_3C	−0.801	0.000	2.028	0.775	0.000	−0.801	2.028	0.775
	0.801					0.801		
HC≡C	−0.801	0.000	2.026	0.757	0.000	−0.801	2.026	0.757
	0.801					0.801		
N≡C	−0.802	0.000	2.032	0.732	0.000	−0.802	2.032	0.732
	0.802					0.802		
(*E*)-IACN	−0.802	0.000	2.038	0.802	0.035	−0.804	2.029	0.711
	0.801		2.027	0.787		0.804		
(*Z*)-IACN	−0.802	0.000	2.034	0.780	0.008	−0.804	2.030	0.718
	0.802		2.031			0.804		
HC=O	−0.797	0.000	2.037	0.854	−0.009	−0.810	2.042	0.623
	0.798		2.045	0.863		0.810		
NH_2	−0.774	0.000	1.972	1.088	−0.010	−0.810	2.023	0.577
	0.777		1.989	1.123		0.810		
O=N	−0.792	0.000	1.983	0.911	−0.021	−0.813	2.006	0.570
	0.797		2.022	0.951		0.813		
N_3	−0.785	0.016	1.990	0.972	0.000	−0.803	2.000	0.658
	0.785					0.807	2.029	0.680

[a] All quantities are in atomic units.

related to the nonlocal response of the small density and to peculiar variations of the substituent field over the target volume. A comparison of the interatomic densities of the nitriles with that of the C≡N⁻ ion shows that the formation of an extra covalent bond depletes M_1 and M_2 and shifts the position of M_1 and the saddle point toward the C while it moves M_2 in the opposite direction. The values of μ_3 for M_1 also are decreased by the covalent and intermediate bond formation showing that the largest maximum has a more "rounded" shape after the charge transfer. Small shifts from the internuclear C–N axis were observed in the position of the maxima and saddle point in all the asymmetric nitriles; the largest being in N=O—C≡N. These shifts show again the perturbation produced by the perpendicular substituent field even on the tightly held C≡N bond density.

In the cyanides, the bond formation increased M_1 with respect to that of the C≡N⁻, while M_2 is reduced in HBe—C≡N and disappears in B—C≡N. These changes are induced by the polarization generated by the counterion[6] and are different if the anion retains only the electron core as in Li^+ or if it has its own bonded and/or nonbonded valence density as in HBe—C≡N or B—C≡N.

The saddle points (see Table VI) found in the N valence shell showed a behavior similar to that of the C atom. In linear nitrile, a circle of (2,0) saddle points was found around the C–N direction, while in the asymmetric ones only two saddle points and two mimima were found in the N valence shell. In the nonlinear nitriles, the values of the $\nabla^2\rho(r)$ and the position of the critical points were a function of the fragment R. The more polar fragments produced the largest shifts indicating again the presence of a transverse field effect. As expected from the increase distance[1,2] from the perturbing center, the changes in the $\nabla^2\rho(r)$ were much less marked in the N than in the C atom.

The distribution of the N "lone pair" showed that, upon additional covalent bond formation, μ_3 and the value of the maximum in the $\nabla^2\rho(r)$ is increased with respect to the C≡N⁻ while its position is shifted toward the N nucleus (see Table VII). These changes are a result of the back-polarization of the N nonbonded density required to compensate the donation of charge of the

Table VII. Position and Laplacian at the Nonbonded Maximum of the N Atom

R	X	Z	$-\nabla^2\rho(r)$	μ_3
C≡N⁻	0.000	3.016	2.872	243.824
HBe	0.000	2.928	3.409	276.041
B	0.000	2.888	3.548	284.175
F	0.000	2.938	3.057	258.710
HO	−0.002	2.938	3.081	259.290
FO	−0.013	2.938	3.196	265.889
H	0.000	2.926	3.359	274.388
H_3C	0.000	2.932	3.238	267.155
HC≡C	0.000	2.934	3.321	272.278
N≡C	0.000	2.939	3.436	278.450
(*E*)-IACN	0.004	2.930	3.329	272.203
(*Z*)-IACN	0.004	2.930	3.341	273.003
HC=O	−0.003	2.942	3.397	275.956
NH_2	−0.009	2.940	3.082	259.314
O=N	−0.016	2.898	3.386	276.409
N_3	−0.011	2.929	3.154	263.549

[a] All quantities are in atomic units.

C≡N⁻ toward R. The position of the N nonbonded density was also slightly shifted from the C–N axis in the asymmetric nitriles being in N=O > FO > N_3 > NH_2 > HC=O = (*E*)-IACN = (*Z*)-IACN. The position along the *Z* axis and the value of the $\nabla^2\rho(r)$ and of μ_3 were slightly different in (*E*)- than in (*Z*)-IACN. This shows that even a small variation in the substituent field may influence $\rho(r)$ far away from the source indicating the long range of the field effect. In the cyanides, μ_3 and the $\nabla^2\rho(r)$ in the N "lone pair" are increased upon bond formation, while the maximum moves toward the N nucleus as in nitriles.

The electrical multipoles of the atoms defined uniquely by the zero-flux surfaces[4-9] provide additional information about more global changes in the C≡N group.[33] The multipoles employed are (a) the total atomic charge, $q(a) = \int_\Omega \rho(r)\, d\upsilon - Z(\alpha)$, where $Z(\alpha)$ is the nuclear charge of atom α and the integral is taken

(33) Hirshfeld, F. L. *Theor. Chim. Acta (Berlin)* **1977**, *44*, 129–138.

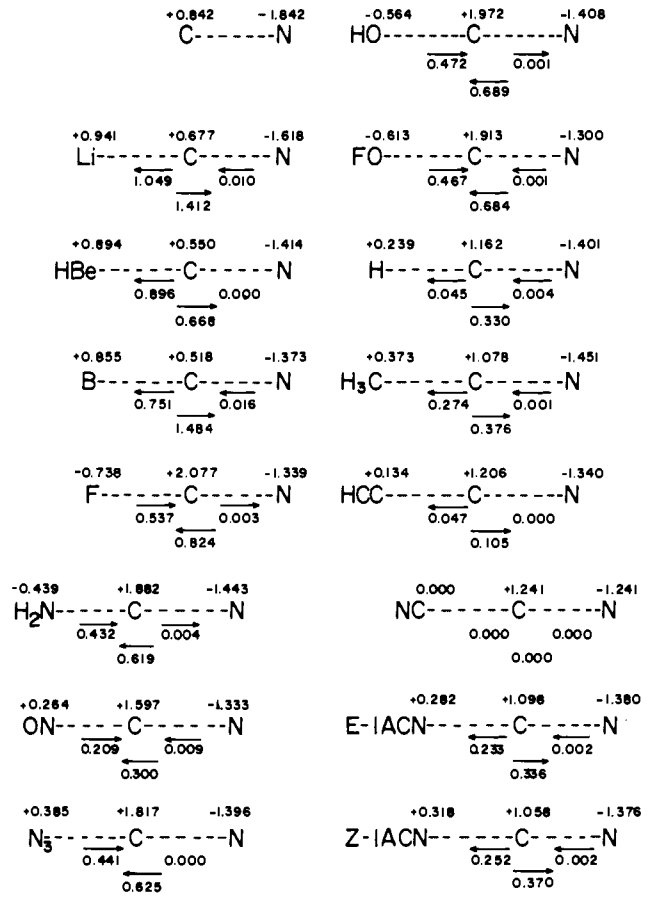

Figure 3. Diagram showing information about the electric multipoles. The value of the charge obtained after integrating within the topologically defined atoms are shown on the top of each atom of the C≡N group and also the total charge of the fragment R is shown at the top left line of each molecule. Below each bond is shown the displacement of its critical point with respect to the position found in the N≡C—C≡N molecule. In the second line below the C atom of the C≡N group, the changes in the Z component of the atomic dipole moment are shown. All the values are in au.

over the atomic volume Ω and (b) the atomic dipole moment, $\mu_i = -\int_\Omega \rho(r) i \, dv$ where $i = x, y$, and z. Figure 3 shows the atomic charges calculated for the C≡N group and the fragment R. The charge transfer to the C≡N fragment approximately reflected ($r = 0.903$) the difference in electronegativities between R and that group although a better correlation was found ($r = 0.948$) with the atomic charge of the target C atom q_C. The charge at the target N atom q_N did not correlate instead with the electronegativity of R as expected from the small changes found in its basin. The donating trend obtained in the atomic charges was Li > HBe > CH_3 > (Z)-IACN > (E)-IACN > HC=O > H > HC≡C, while for the withdrawing one it was F > FO > HO > NH_2 > N_3 > N=O. From Figure 3, we see that q_N is more sensitive to the change in the substituent than the position of the critical point of the C≡N bond. The changes in q_N contain two contributions: one arising from the change in the density within the basin of the unperturbed atom and another from the changes in volume of the basin as it is perturbed.[34] The small variations found in $S_{C\equiv N}$ show that the changes in q_N are associated mainly with the changes in the density within the N basin than with the variation in the $S_{C\equiv N}$ surface itself.

Table VIII. Components X and Z of the Atomic Dipole Moment of the C≡N Group

	C		N	
R	⟨X⟩	⟨Z⟩	⟨X⟩	⟨Z⟩
C≡N⁻	0.000	1.990	0.000	1.039
Li	0.000	2.257	0.000	1.048
B	0.000	1.513	0.000	1.006
F	0.000	0.021	0.000	0.816
HO	−0.024	0.156	−0.003	0.885
FO	0.060	0.161	−0.010	0.850
H	0.000	1.096	0.000	0.972
H_3C	0.000	1.221	0.000	0.955
HC≡C	0.000	0.950	0.000	0.887
N≡C	0.000	0.845	0.000	0.872
(E)-IACN	−0.027	1.181	−0.011	0.932
(Z)-IACN	−0.027	1.215	−0.003	0.935
HC=O	0.032	1.169	0.009	0.914
NH_2	−0.017	0.226	−0.001	0.886
O=N	0.109	0.545	−0.016	0.912
N_3	0.018	0.220	−0.005	0.872

[a] All quantities are in atomic units.

The atomic dipole moment[34] provides a measure of the departure of the centroid of negative charge from the nuclear center. In Table VIII are shown the values of ⟨Z⟩ and ⟨X⟩ calculated for the C≡N group in different nitriles and cyanides with the Z axis taken along the C–N direction. The values of ⟨Y⟩ were very small, indicating that the atomic dipoles had only components in the XZ (nuclear) plane and are not shown. We see from Table VIII that the values of the ⟨Z⟩ and ⟨X⟩ components of the C atom vary over a much wider range than in the N atom confirming that the C atom suffers most of the changes upon the R–C bond formation. On the other hand, the high polarity of C≡N group is such that the ⟨Z⟩ is the more important component in the atomic dipole moment in both atoms. A regression analysis showed that, with cyanogen as a reference, the variation of the ⟨Z⟩ component $\Delta\langle Z\rangle_c$ was related ($r = 0.992$) with the changes in the position of the critical point Δr_c in the C atom. The correlation shows that a fragment that withdraws electron density from the C atom pushes the bond critical point toward this atom and leads to a polarization of the density in a direction opposite to that of Δr_c. An opposite behavior for ⟨Z⟩ was found for electron-donating fragments as also seen in Figure 3. For asymmetric nitriles, the values of the ⟨X⟩ component of the dipole in both atoms of the target group are small but finite, showing again the effect of the perpendicular field on the C charge distribution already noted in other extremes of the target valence shells.

Conclusions

The topological analysis of the electron densities of the C≡N target group in nitriles and cyanides showed that subtle substituent effects can be determined directly in the three-dimensional space through the study of the extremes of the $\nabla^2\rho(r)$ distribution of the target valence shells and that the bonding between the C≡N group and a fragment R can be unequivocally characterized by the values of $\rho(r)$ and $\nabla^2\rho(r)$ at the bond critical point.

Acknowledgment. We thank the Centro Cientifico of IBM de Venezuela C.A. for a generous grant of computer time, to J. Rivero and J. A. Rodriguez for their valuable help with the graphic programs and to R. Bonaccorsi from Istituto di Chimica Quantistica ed Energetica Molecolare del C.N.R., Pisa, Italy, for providing a copy of the MONSTERGAUSS program.

(34) Slee, T.; Larouche, A.; Bader, R. F. W. *J. Phys. Chem.* **1988**, *92*, 6219–6227.